

Photonic Crystal Optical Parametric Oscillator

Gabriel Marty^{1,2}, Sylvain Combrié¹, Fabrice Raineri^{2,3}, Alfredo De Rossi^{1,*}

¹ *Thales Research and Technology, Campus Polytechnique,
1 avenue Augustin Fresnel, 91767 Palaiseau, France*

² *Centre de Nanosciences et de Nanotechnologies,
CNRS, Université Paris Saclay, Palaiseau, France*

³ *Université de Paris, 5 Rue Thomas Mann, 75013 Paris, France*

* *Corresponding author: alfredo.derossi@thalesgroup.com*

Abstract

Miniaturization of devices has been a primary objective in microelectronics and photonics for decades, aiming at denser integration, enhanced functionalities and drastic reduction of power consumption. Headway in nanophotonics is currently linked to the progress in concepts and technologies necessary for applications in information and communication[1], brain inspired computing[2], medicine and sensing[3] and quantum information[4]. Amongst all nanostructures, semiconductor photonic crystals (PhCs) [5] occupy a prominent position as they enable the fabrication of quasi ultimate optical cavities[6]. Low threshold laser diodes[7, 8] or Raman lasers[9], low power consuming optical memories[10], efficient single photon sources [11] or single photon quantum gates[12] are impressive examples of their capabilities.

We report the demonstration of a $\approx 20\mu\text{m}$ long PhC semiconductor optical parametric oscillator (OPO) at telecom wavelength exploiting nearly diffraction limited optical modes. The pump power threshold is measured below $200\mu\text{W}$. Parametric oscillation was reached through the drastic enhancement of Kerr optical Four Wave Mixing by thermally tuning the high Q modes of a nanocavity into a triply resonant configuration. Miniaturization of this paradigmatic source of coherent light paves the way for quantum optical circuits, dense integration of highly efficient nonlinear sources of squeezed light or entangled photons pairs.

Optical Parametric Oscillators (OPO) are sources of coherent light relying on the ultra-fast nonlinear response of matter for the stimulated emission of photon pairs. OPOs can generate light within a spectral range only limited by the transparency of the nonlinear material. Consequently, they are broadly used in spectroscopy[13]. As the generated photons are correlated, OPOs are also sources of nonclassical light for quantum optics[14, 15] and quantum computing[16]. OPOs are typically available as solid state optical devices, tending to be bulky and expensive. Their miniaturization is crucial for their deployment in photonic integrated circuits, e.g. for optical interconnects[17, 18]. This challenging task can only be tackled by increasing power efficiency of the involved nonlinear effects in order to keep on-chip optical power as low as possible. Low power levels can be reached through the resonant enhancement of the interacting waves in high Q cavities. High-Q and low mode volumes are the two critical cavity parameters to decrease the power threshold for parametric oscillation[19]. The exceptional progress in the development of high-Q microresonators has enabled smaller and more practical OPOs[20, 21]. In order to obtain even more compact devices, the use of nanocavities made of highly nonlinear material, such as semiconductors, seems to be the appropriate answer. High-Q resonances with diffraction-limited mode volumes $\approx (\lambda/n)^3$, with n the refractive index, are possible in a Photonic Crystal (PhC) cavity[5, 6]. Although the possibility of a PhC OPO was considered theoretically more than a decade ago[22, 23], the demonstration is extremely challenging and still missing.

Our PhC OPO relies on harnessing triply resonant degenerate Four Wave Mixing (FWM) (see Fig. 1(a)). For this Kerr optical nonlinear process, energy conservation dictates the relation between the pump and the generated photons ($2\omega_p = \omega_i + \omega_s$), meaning that the new frequencies ω_i and ω_s are generated symmetrically with respect to the pump one ω_p . Thus, resonant enhancement is only possible if three cavity eigenfrequencies ($\omega_0, \omega_+, \omega_-$) are rigorously equispaced. This condition is in general not satisfied in PhC resonators. Here, tight localization of light is related to the existence of forbidden bands in the optical spectrum[24, 25]. In contrast to Fabry-Perot or ring resonators, PhC cavities can be designed to support a very small number of modes. Triply resonant parametric interaction was observed in a system made of three coupled PhC nanocavities with a limited efficiency due to low Q factor[26]. Similar experiments were performed in ultrahigh-Q coupled resonators waveguides[27] but did not lead to the expected drastic enhancement of the parametric

interaction, likely because the eigenfrequencies were not equally spaced. In fact, the control of the frequency spacing is ultimately limited by structural disorder: even in state-of-the-art PhC technology, resonances deviate from their design value by about 40 GHz [28]. For this reason, in absence of a tuning mechanism, the eigenmode linewidth must be large enough to allow triply resonant FWM. This corresponds to $Q < 5 \times 10^3$, clearly hindering the opportunity offered by PhC[6].

In this work, we demonstrate a PhC OPO operated at ultra-low power. This result was achieved owing to three key features: first, we designed the cavity to have equispaced eigenfrequencies, then, we introduced a differential thermo-refractive tuning mechanism to compensate for the residual spectral misalignment caused by fabrication imperfections and, finally, we used $\text{In}_{0.5}\text{Ga}_{0.5}\text{P}$ III- V semiconductor as the constitutive material of our cavity. The large electronic bandgap of this material enables the mitigation of Two Photon Absorption (TPA)[29] which otherwise clamps nonlinear conversion efficiency below parametric oscillations.

The PhC cavity[30] is designed to create an effective parabolic potential for the optical field, Fig. 1(b), such that eigenfrequencies are equispaced and the eigenmodes correspond to Gauss-Hermite (GH) functions. The design (Fig. 1(c)) consists of a suspended membrane with a regular hexagonal lattice of holes with period a , except for a line of missing holes, where light can propagate. There, we introduce a bichromatic lattice[31], by modifying the period a' of the innermost row of holes. The localization of the field and the Free Spectral Range (FSR) between higher order modes are controlled by the commensurability parameter a'/a . Choosing $a'/a = 0.98$ corresponds to a FSR about 400 GHz and the field envelopes are very close to GH functions, Fig. 1(b). The optical access to the modes is provided by a single-ended waveguide on the side terminated with a mode adapter to maximize coupling to an optical fiber[32].

Our fabrication process ineluctably induces fluctuations on the targeted eigenfrequencies that result in a misalignment (50 GHz on average) far greater than the resonance linewidth (inferior to 1 GHz)[33]. Thermal tuning can compensate for this deviation: a section of the cavity is heated to locally increase the refractive index of the material, hence the resonant

wavelength of the modes[34]. When it is done on a smaller scale than the spatial extension of the targeted set of modes, each of them will spectrally shift differently and relatively to their overlap with the temperature gradient. Local heating can be realized through the projection on the sample surface of a patterned incoherent pumping beam[35], this method being limited by the precision of the projection system. In our work, the tuning of three modes of a single cavity is automatically achieved by resonantly injecting light at mode "0", also used as the "pump" mode for the FWM process. A temperature gradient following the intensity mode distribution is created inside the cavity through residual optical absorption. As can be seen in Fig. 1(b), the GH modes exhibits different spatial profiles, inducing inhomogeneous spectral shifts. When the pump laser at ω_p is swept from blue to red across the resonance, mode "0" redshifts from $\bar{\omega}_0$ (cold) to ω_0 (hot). The spectral evolution of the pump, and the modes at ω_+ and ω_- involved in the FWM process are represented in Fig.1(d). The different modes shift differently as expected. The misalignment of the hot cavity $2\Delta_\chi = 2\omega_0 - \omega_- - \omega_+$ is deduced from these measurements and is found to be $2\Delta_\chi = 2\bar{\Delta}_\chi + 0.48\Delta_0$ where $\bar{\Delta}_\chi$ is the misalignment of the "cold" cavity and $\Delta_0 = \omega_p - \bar{\omega}_0$ is the pump offset. This shows that an originally mismatched triplet can eventually be aligned by adjusting the pump frequency, which is clearly observed in Fig.1(e) where the two considered FSRs are equalized (crossing of blue and red lines).

We now investigate the impact of the triple resonance condition on the parametric gain. This dependence is deduced from stimulated FWM experiments, where an additional laser ("signal") at ω_s is swept across the resonance at ω_- when the pump frequency is fixed. An idler wave is generated at $\omega_i = 2\omega_p - \omega_s$. As a matter of fact, the stimulated efficiency $\eta_\chi = P_i/P_s$, defined as the ratio between the output idler power (P_i) over the input signal power (P_s), is directly related to the parametric gain and the loss of the cavity. Parametric oscillation is reached when the gain is high enough to compensate for the loss, corresponding to the asymptotic limit of $\eta_\chi \rightarrow 1$. The measured values of η_χ for a sample with an average Q[36] of about 7×10^4 are displayed on Fig. 2(a) as a function of the pump offset for an input pump power of $700 \mu\text{W}$. η_χ peaks at 0.4 % (-25dB) when $\Delta_0/2\pi = -110\text{GHz}$, in agreement with the triply resonant configuration predicted by our thermal tuning measurements shown Fig. 2(b). To support these results, an analytical model (see Supplementary Information Section I) is derived and η_χ writes, in the limit of undepleted pump and low parametric gain, as:

$$\eta_\chi = \eta_\chi^{(max)} \mathcal{L}\left(\frac{\delta_0}{\Gamma_0}\right)^2 \mathcal{L}\left(\frac{\delta_-}{\Gamma_-}\right) \mathcal{L}\left(\frac{\delta_+}{\Gamma_+}\right) \quad (1)$$

where $\delta_0 = \omega_p - \omega_0$, $\delta_- = \omega_s - \omega_-$, $\delta_+ = \omega_i - \omega_+$ are the frequency detunings of the pump, signal and idler with respect to the hot resonances. Γ_0 and Γ_- , Γ_+ are the photon damping rates in the corresponding modes ($\Gamma = \omega/Q$). $\mathcal{L}(x)$ is the Lorentzian function. $\eta_\chi^{(max)}$ is the maximum achievable efficiency obtained when the triplet is aligned and when the waves frequencies correspond to the resonant modes ($\delta_0 = \delta_- = \delta_+ = 0$). The calculated map of η_χ versus the pump offset and probe detuning δ_- reveals two local maxima merging into an absolute maximum of efficiency, corresponding to a perfectly aligned cavity (Fig. 2(b)). Remarkably, the measurements are in quantitative agreement with our model (see Inset of Fig.2(a)) plugged with parameters either calculated or measured, and the intracavity power adjusted by less than 10% to account for experimental uncertainties (more details in the Supplementary Information Section II).

Thanks to our thermal tuning technique, higher FWM efficiencies are within reach by working with cavities exhibiting higher Qs even though the resonance linewidth become narrower. We performed stimulated FWM on a sample with an average $Q = 1.2 \times 10^5$. It results in a drastic improvement of the efficiency that rises up to 26 % (- 5.8 dB) with an on chip pump power of 80 μ W (Fig 2(c)) and Fig 2(d)). The scaling of efficiency with Q is detailed in the Supplementary Information Section I.(F). We also note that the dependence of the efficiency on the probe detuning, Fig. 2(c), is very sharp, because of the triple resonant enhancement of FWM.

In these samples, parametric oscillation is not observed, meaning that the maximum realizable parametric gain is not sufficient to compensate for cavity loss. This value is entirely determined by the cavity optical properties (Q, mode volume, nonlinear cross-section, material nonlinearity) and the pump power level required to align the three modes. Its value is therefore unique for each triplet of modes. Eventually, parametric oscillation is demonstrated for a resonator with $Q_{avg} \approx 2.5 \times 10^5$. The sample is pumped with an on-chip power level below 200 μ W, which is enough to align a triplet of adjacent resonances. As the pump offset $\Delta_0/2\pi < -170$ GHz, the red ω_- and blue ω_+ signals emerge from noise (-73 dBm = 50 pW), as can shown in Fig.3(a). When approaching -175 GHz, they abruptly increase by four orders of magnitude, a clear indication of an oscillation threshold. Interestingly, the pump

offset, is, to a good approximation directly proportional to the energy stored in the pump mode as the spectral shift is induced by linear absorption. Therefore, the result can be cast in a more familiar representation by estimating the equivalent pump power circulating in the cavity $P_{c,0}$ (see Supplementary Information section III.A) in Fig.3(b). Above threshold $P_{c,0} > P_{th} = 175\mu W$, the on-chip generated power increases linearly with $P_{c,0} - P_{th}$. More than 50% of the excess pump power is converted. Strikingly, the threshold expected from our model is $170\mu W$ (see Supplementary Table III). As the detuning is further increased, the parametric oscillation shuts off at $\Delta_0/2\pi = -183\text{GHz}$, although the pump mode is still on resonance. The cavity is now misaligned.

The performance of our ultracompact system based on interacting standing waves is already comparable to that of recently demonstrated semiconductor microring and racetrack OPOs which exhibits power thresholds between 3 and 25 mW, as shown in Fig.3(c). The very low power threshold of our PhC OPO results from the strong confinement of the interacting modes, the large nonlinearity of semiconductors and a moderately large Q factor. The mode volumes of about $0.2\mu m^3$, are 150 times smaller than in ring resonators with comparable FSR [37]. So far, lower power thresholds were observed very recently[38] in AlGaAs based microring ($36\mu W$), thanks to larger the nonlinearity of the material, much higher Qs and larger FSR. Lower values (down to $5\mu W$) are only reported in non-integrated and non-semiconductor resonators that require highly optimized fabrication process[39] and second order nonlinearity. Considering that current state-of-the art PhC cavities[6] exhibit $Q > 10^7$, OPOs with power thresholds below the μW level can be realistically considered.

As in any other laser source, power threshold is not the sole figure of merit. Also the overall energy efficiency transfer from the pump to the side modes is crucial. In our case, the estimated total generated power, when considering outcoupling loss (7dB) is about $5\mu W$ (measurement is in Supplementary Information section II.B), leading to a conversion efficiency which is about 2.5% of the coupled pump power. This value can be compared to the one of 17 % very recently reported in AlN ring resonators[40], which are operated at much larger power (10 mW) and exploit the $\chi^{(2)}$ nonlinearity. However, the PhC OPO measured slope efficiency (signal+idler) is above 50%, indicating that a much better overall efficiency is possible by optimizing the coupling to the feeding waveguide.

Finally, it is interesting to point out that our OPO behaves as a pure degenerate parametric system with only three cavity modes interacting. Simultaneous alignment of more than one

triplet is very unlikely. This is apparent in Fig. 1(e), where another triplet (x , $+$ and 0) is aligned at a different pump offset $\Delta_0 \approx 50$ GHz. This characteristic, possible in ring resonator with a sophisticated sidewall corrugation[41], could find an application in laser noise reduction[42]. For the same reason, resonant nonlinear contributions such as Raman can be ignored, unless the resonator is deliberately designed for, as in Ref. [9].

In conclusion, we achieved a low-power operating OPO with a footprint far smaller than other competing approaches. It is of particular interest when it comes to considering incorporation within sophisticated optical circuits[43]. This demonstration opens up exciting avenues for building an integrated all semiconductor platform to optically generate and process both classical and quantum data.

METHODS

The cavities are suspended membranes made of Indium Gallium Phosphide lattice-matched to GaAs. The photonic crystal is created using e-beam lithography, dry etch of the hard mask, inductively coupled plasma etching of the holes and wet etching of the underlying material substrate to release the membrane[44]. The large electronic gap (1.89 eV) prevents two-photon absorption when operating the telecom spectral band, while the residual absorption rate $\Gamma_{abs} = 2 \times 10GHz$ is very low[45]. Optical measurements have been performed on a temperature stabilized sample holder position stage and the two-way optical access is provided by a microscope objective lensed fiber, actuated by a 3-axis nanopositioner stage, and a circulator. A tunable laser source is connected to the sample through a variable attenuator and the output is directly fed to the Optical Spectrum Analyzer.

-
- [1] Chen Sun, Mark T Wade, Yunsup Lee, Jason S Orcutt, Luca Alloatti, Michael S Georgas, Andrew S Waterman, Jeffrey M Shainline, Rimas R Avizienis, Sen Lin, et al. Single-chip microprocessor that communicates directly using light. *Nature*, 528(7583):534–538, 2015.
- [2] J Feldmann, N Youngblood, CD Wright, H Bhaskaran, and WHP Pernice. All-optical spiking neurosynaptic networks with self-learning capabilities. *Nature*, 569(7755):208–214, 2019.
- [3] M Carmen Estevez, Mar Alvarez, and Laura M Lechuga. Integrated optical devices for lab-on-a-chip biosensing applications. *Laser & Photonics Reviews*, 6(4):463–487, 2012.
- [4] Lucia Caspani, Chunle Xiong, Benjamin J Eggleton, Daniele Bajoni, Marco Liscidini, Matteo Galli, Roberto Morandotti, and David J Moss. Integrated sources of photon quantum states based on nonlinear optics. *Light: Science & Applications*, 6(11):e17100, 2017.
- [5] Yoshihiro Akahane, Takashi Asano, Bong-Shik Song, and Susumu Noda. High-Q photonic nanocavity in a two-dimensional photonic crystal. *Nature*, 425(6961):944–947, 2003.
- [6] Takashi Asano, Yoshiaki Ochi, Yasushi Takahashi, Katsuhiko Kishimoto, and Susumu Noda. Photonic crystal nanocavity with a Q factor exceeding eleven million. *Optics Express*, 25(3):1769, 2017.
- [7] Kengo Nozaki, Shinji Matsuo, Takuro Fujii, Koji Takeda, Akihiko Shinya, Eiichi Kuramochi, and Masaya Notomi. Femtofarad optoelectronic integration demonstrating energy-saving signal conversion and nonlinear functions. *Nature Photonics*, page 1, 2019.
- [8] Guillaume Crosnier, Dorian Sanchez, Sophie Bouchoule, Paul Monnier, Gregoire Beaudoin, Isabelle Sagnes, Rama Raj, and Fabrice Raineri. Hybrid Indium Phosphide-on-Silicon nanolaser diode. *Nature Photonics*, 11(5):297, 2017.
- [9] Yasushi Takahashi, Yoshitaka Inui, Masahiro Chihara, Takashi Asano, Ryo Terawaki, and Susumu Noda. A micrometre-scale raman silicon laser with a microwatt threshold. *Nature*, 498(7455):470, 2013.
- [10] Kengo Nozaki, Akihiko Shinya, Shinji Matsuo, Yasumasa Suzaki, Toru Segawa, Tomonari Sato, Yoshihiro Kawaguchi, Ryo Takahashi, and Masaya Notomi. Ultralow-power all-optical ram based on nanocavities. *Nature Photonics*, 6(4):248, 2012.
- [11] Peter Lodahl, Sahand Mahmoodian, and Søren Stobbe. Interfacing single photons and single quantum dots with photonic nanostructures. *Reviews of Modern Physics*, 87(2):347, 2015.

- [12] Shuo Sun, Hyochul Kim, Zhouchen Luo, Glenn S. Solomon, and Edo Waks. A single-photon switch and transistor enabled by a solid-state quantum memory. *Science*, 361(6397):57–60, 2018.
- [13] Frank K Tittel, Dirk Richter, and Alan Fried. Mid-infrared laser applications in spectroscopy. In *Solid-state mid-infrared laser sources*, pages 458–529. Springer, 2003.
- [14] Olivier Morin, Virginia D’Auria, Claude Fabre, and Julien Laurat. High-fidelity single-photon source based on a type ii optical parametric oscillator. *Opt. Lett.*, 37(17):3738–3740, 2012.
- [15] Olivier Morin, Kun Huang, Jianli Liu, Hanna Le Jeannic, Claude Fabre, and Julien Laurat. Remote creation of hybrid entanglement between particle-like and wave-like optical qubits. *Nature Photonics*, 8(7):570, 2014.
- [16] Takahiro Inagaki, Kensuke Inaba, Ryan Hamerly, Kyo Inoue, Yoshihisa Yamamoto, and Hiroki Takesue. Large-scale ising spin network based on degenerate optical parametric oscillators. *Nature Photonics*, 10(6):415–419, 2016.
- [17] Jacob S Levy, Alexander Gondarenko, Mark A Foster, Amy C Turner-Foster, Alexander L Gaeta, and Michal Lipson. Cmos-compatible multiple-wavelength oscillator for on-chip optical interconnects. *Nature photonics*, 4(1):37–40, 2010.
- [18] L Razzari, D Duchesne, M Ferrera, R Morandotti, S Chu, BE Little, and DJ Moss. Cmos-compatible integrated optical hyper-parametric oscillator. *Nature Photonics*, 4(1):41–45, 2010.
- [19] Andrey B. Matsko, Anatoliy A. Savchenkov, Dmitry Strekalov, Vladimir S. Ilchenko, and Lute Maleki. Optical hyperparametric oscillations in a whispering-gallery-mode resonator: Threshold and phase diffusion. *Physical Review A*, 71(3), 2005.
- [20] TJ Kippenberg, SM Spillane, and KJ Vahala. Kerr-nonlinearity optical parametric oscillation in an ultrahigh-q toroid microcavity. *Physical review letters*, 93(8):083904, 2004.
- [21] Ivan S Grudinin, Andrey B Matsko, Anatoliy A Savchenkov, Dmitry Strekalov, Vladimir S Ilchenko, and Lute Maleki. Ultra high q crystalline microcavities. *Optics Communications*, 265(1):33–38, 2006.
- [22] Claudio Conti, Andrea Di Falco, and Gaetano Assanto. Optical parametric oscillations in isotropic photonic crystals. *Optics express*, 12(5):823–828, 2004.
- [23] David M. Ramirez, Alejandro W. Rodriguez, Hila Hashemi, J. D. Joannopoulos, Marin Soljačić, and Steven G. Johnson. Degenerate four-wave mixing in triply resonant Kerr cavities. *Physical Review A*, 83(3), 2011.

- [24] Sajeev John. Strong localization of photons in certain disordered dielectric superlattices. *Physical Review Lett.*, 58(23):2486–2489, 1987.
- [25] Eli Yablonovitch. Inhibited spontaneous emission in solid-state physics and electronics. *Physical review letters*, 58(20):2059, 1987.
- [26] Stefano Azzini, Davide Grassani, Matteo Galli, Dario Gerace, Maddalena Patrini, Marco Liscidini, Philippe Velha, and Daniele Bajoni. Stimulated and spontaneous four-wave mixing in silicon-on-insulator coupled photonic wire nano-cavities. *Applied Physics Letters*, 103(3):031117, 2013.
- [27] Nobuyuki Matsuda, Eiichi Kuramochi, Hiroki Takesue, Kaoru Shimizu, and Masaya Notomi. Resonant photon pair generation in coupled silicon photonic crystal nanocavities. In *The European Conference on Lasers and Electro-Optics*, page CK.8.4. Optical Society of America, 2017.
- [28] Yuki Taguchi, Yasushi Takahashi, Yoshiya Sato, Takashi Asano, and Susumu Noda. Statistical studies of photonic heterostructure nanocavities with an average Q factor of three million. *Optics Express*, 19(12):11916, June 2011.
- [29] Pierre Colman, Chad Husko, Sylvain Combrié, Isabelle Sagnes, Chee Wei Wong, and Alfredo De Rossi. Temporal solitons and pulse compression in photonic crystal waveguides. *Nature Photonics*, 4(12):862–868, 2010.
- [30] Sylvain Combrié, Gaëlle Lehoucq, Grégory Moille, Aude Martin, and Alfredo De Rossi. Comb of high-Q resonances in a compact photonic cavity. *Laser & Photonics Reviews*, 11(6):1700099, 2017.
- [31] Filippo Alpeggiani, Lucio Claudio Andreani, and Dario Gerace. Effective bichromatic potential for ultra-high Q-factor photonic crystal slab cavities. *Applied Physics Lett.*, 107(26):261110, 2015.
- [32] Quynh Vy Tran, Sylvain Combrié, Pierre Colman, and Alfredo De Rossi. Photonic crystal membrane waveguides with low insertion losses. *Appl. Phys. Lett.*, 95(6):061105, 2009.
- [33] standard deviation over about 300 resonances in 72 resonators is 50 GHz, while linewidth of the resonances is as narrow as about 300 MHz, [30].
- [34] Tal Carmon, Lan Yang, and Kerry J. Vahala. Dynamical thermal behavior and thermal self-stability of microcavities. *Opt. Express*, 12(20):4742–4750, Oct 2004.

- [35] Emre Yüce, Jin Lian, Sergei Sokolov, Jacopo Bertolotti, Sylvain Combrié, Gaëlle Lehoucq, Alfredo De Rossi, and Allard P. Mosk. Adaptive control of necklace states in a photonic crystal waveguide. *ACS photonics*, 5(10):3984–3988, 2018.
- [36] $Q_{avg} = (Q_0^2 Q_- Q_+)^{1/4}$.
- [37] $V_m = 30\mu m^3$ for FSR = 500 GHz[46] Considering the interaction volume $V_\chi = 5.7\mu m^3$, this is still an order of magnitude smaller than $V_{\chi,ring} = 1.54 \times 2\pi A_{eff} L = 50\mu m^3$.
- [38] Lin Chang, Weiqiang Xie, Haowen Shu, Qifan Yang, Boqiang Shen, Andreas Boes, Jon D Peters, Warren Jin, Songtao Liu, Gregory Moille, et al. Ultra-efficient frequency comb generation in algaas-on-insulator microresonators. *arXiv preprint arXiv:1909.09778*, 2019.
- [39] JU Füst, DV Strekalov, D Elser, A Aiello, Ulrik Lund Andersen, Ch Marquardt, and G Leuchs. Low-threshold optical parametric oscillations in a whispering gallery mode resonator. *Physical Review Letters*, 105(26):263904, 2010.
- [40] Alexander W. Bruch, Xianwen Liu, Joshua B. Surya, Chang-Ling Zou, and Hong X. Tang. On-chip $\chi^{(2)}$ microring optical parametric oscillator. *Optica*, 6(10):1361–1366, 2019.
- [41] Xiyuan Lu, Qing Li, Daron A Westly, Gregory Moille, Anshuman Singh, Vikas Anant, and Kartik Srinivasan. Chip-integrated visible–telecom entangled photon pair source for quantum communication. *Nature physics*, 15(4):373–381, 2019.
- [42] Andrey B. Matsko. Hyperparametric frequency noise eater. *Physical Review A*, 99(2):023843, 2019.
- [43] Gabriel Marty, Sylvain Combrié, Alfredo De Rossi, and Fabrice Raineri. Hybrid InGaP nanobeam on silicon photonics for efficient four wave mixing. *APL Photonics*, 4(12):120801, 2019.
- [44] Sylvain Combrié, Quynh Vy Tran, Alfredo De Rossi, Chad Husko, and Pierre Colman. High quality GaInP nonlinear photonic crystals with minimized nonlinear absorption. *Appl. Phys. Lett.*, 95(22):221108, 2009.
- [45] Inès Ghorbel, François Swiadek, Rui Zhu, Daniel Dolfi, Gaëlle Lehoucq, Aude Martin, Grégory Moille, Loïc Morvan, Rémy Braive, Sylvain Combrié, and Alfredo De Rossi. Optomechanical gigahertz oscillator made of a two photon absorption free piezoelectric III/V semiconductor. *APL Photonics*, 4(11):116103, 2019.
- [46] Minhao Pu, Luisa Ottaviano, Elizaveta Semenova, and Kresten Yvind. Efficient frequency comb generation in algaas-on-insulator. *Optica*, 3(8):823–826, 2016.

- [47] Dalziel J Wilson, Katharina Schneider, Simon Hönl, Miles Anderson, Yannick Baumgartner, Lukas Czornomaz, Tobias J Kippenberg, and Paul Seidler. Integrated gallium phosphide nonlinear photonics. *Nature Photonics*, pages 1–6, 2019.
- [48] BJM Hausmann, I Bulu, V Venkataraman, P Deotare, and Marko Lončar. Diamond nonlinear photonics. *Nature Photonics*, 8(5):369, 2014.
- [49] Austin G Griffith, Ryan KW Lau, Jaime Cardenas, Yoshitomo Okawachi, Aseema Mohanty, Romy Fain, Yoon Ho Daniel Lee, Mengjie Yu, Christopher T Phare, Carl B Poitras, et al. Silicon-chip mid-infrared frequency comb generation. *Nature communications*, 6:6299, 2015.
- [50] Xianwen Liu, Changzheng Sun, Bing Xiong, Lai Wang, Jian Wang, Yanjun Han, Zhibiao Hao, Hongtao Li, Yi Luo, Jianchang Yan, et al. Integrated high-q crystalline aln microresonators for broadband kerr and raman frequency combs. *ACS Photonics*, 5(5):1943–1950, 2018.

Supplementary Information is available in the online version of the paper.

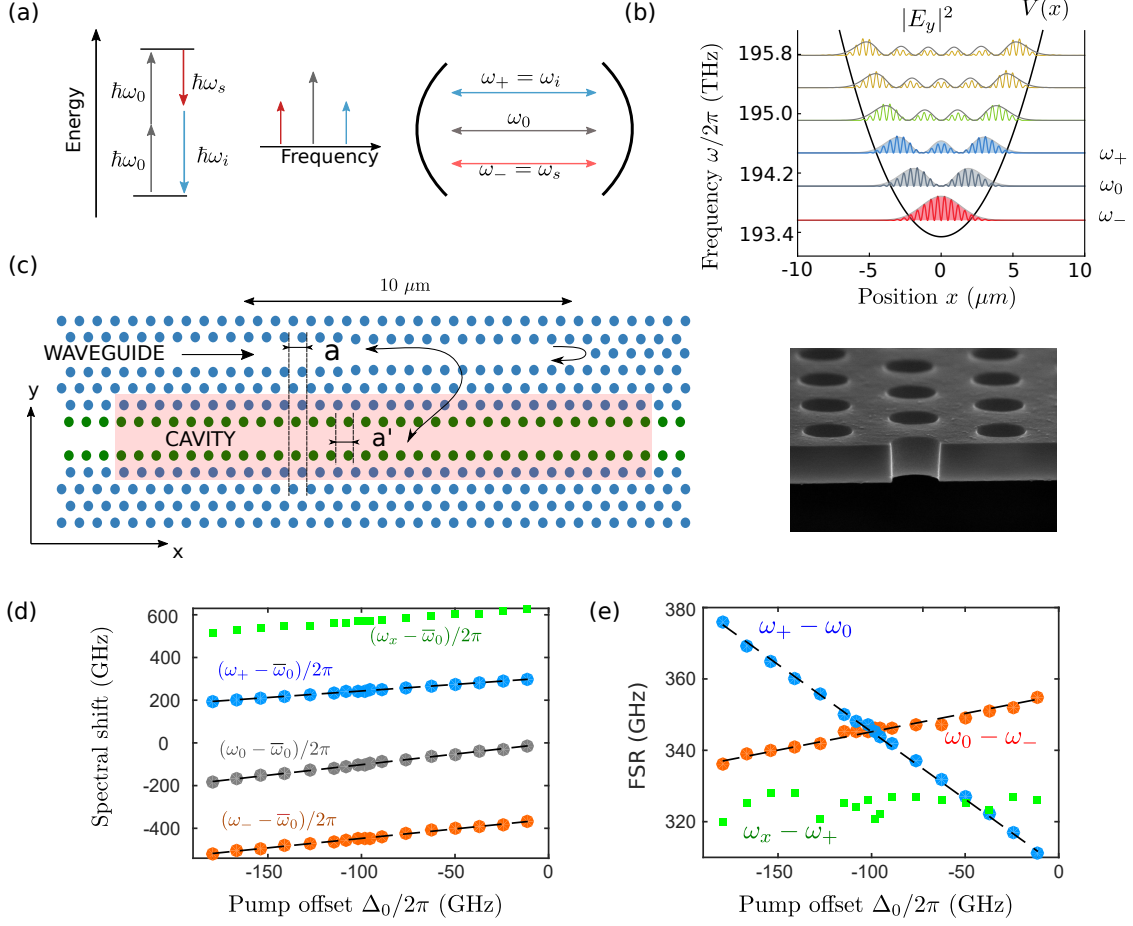


FIG. 1. (a) Concept of the triply-resonant degenerate OPO where resonant modes respect the energy conservation $2\hbar\omega_0 = \hbar\omega_+ + \hbar\omega_-$; (b) calculated Hermite-Gauss modes corresponding to an effective parabolic potential for photons (gray solid lines) and eigenmode frequencies and field amplitudes (color lines) of the bichromatic photonic crystal cavity; the filled curves denote a triplet of interacting modes; (c) Device layout with periods a and a' and access waveguide and SEM image of the InGaP membrane; (d) measured frequencies of the first 4 modes (relative to cold resonance $\bar{\omega}_0$) as a function of the pump offset Δ_0 and linear fit (dashed); (e) corresponding eigenfrequency intervals (FSR)

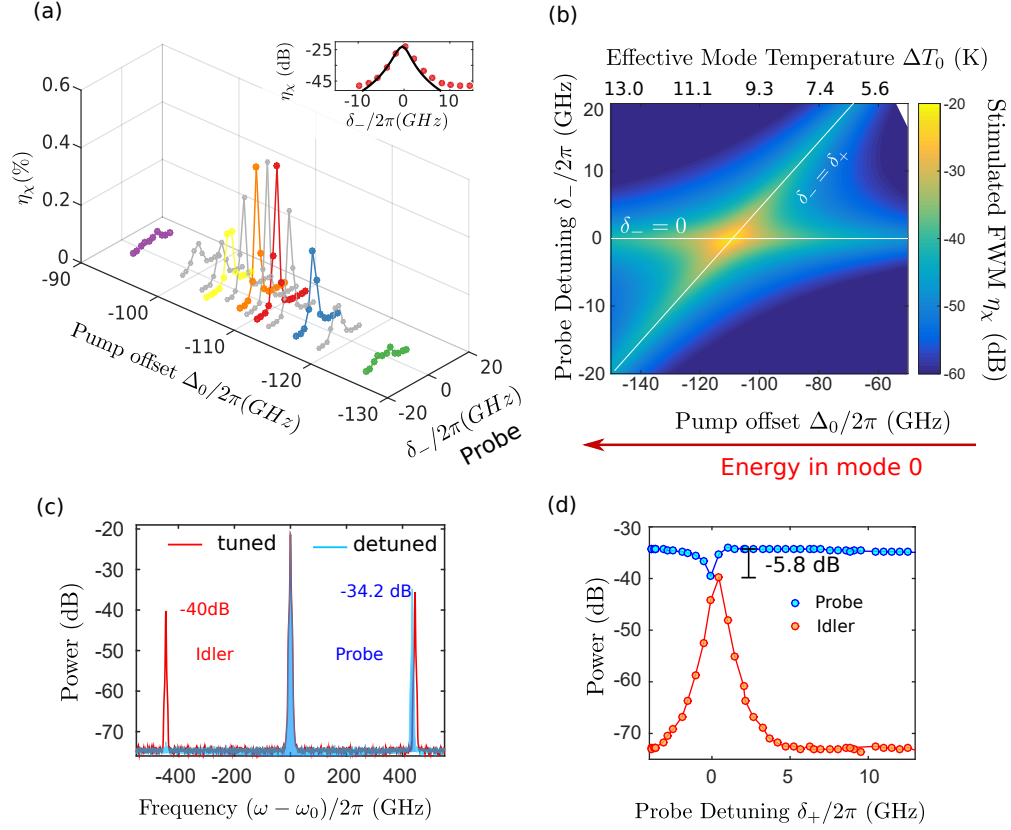


FIG. 2. (a) Measured stimulated FWM efficiency η_χ as a function of the pump offset Δ_0 and probe detuning δ_- ; (Inset) Comparison with the theory (black line) for the red curve. (see Supplementary Fig.S2 for full comparison) (b) Calculated false color map of the efficiency η_χ of stimulated FWM as a function of the probe detuning δ_- and pump offset with corresponding effective mode temperature rise ΔT_0 for mode 0. The white lines represent the poles of eq. 1.(c) Stimulated FWM in a resonator with larger Q_{avg} . Raw spectra centered on the pump ω_0 as a function of the probe detuning δ_- spectra for tuned (red) and detuned (blue) probe; (d) reflected probe (blue) and idler (red) power vs. probe detuning.

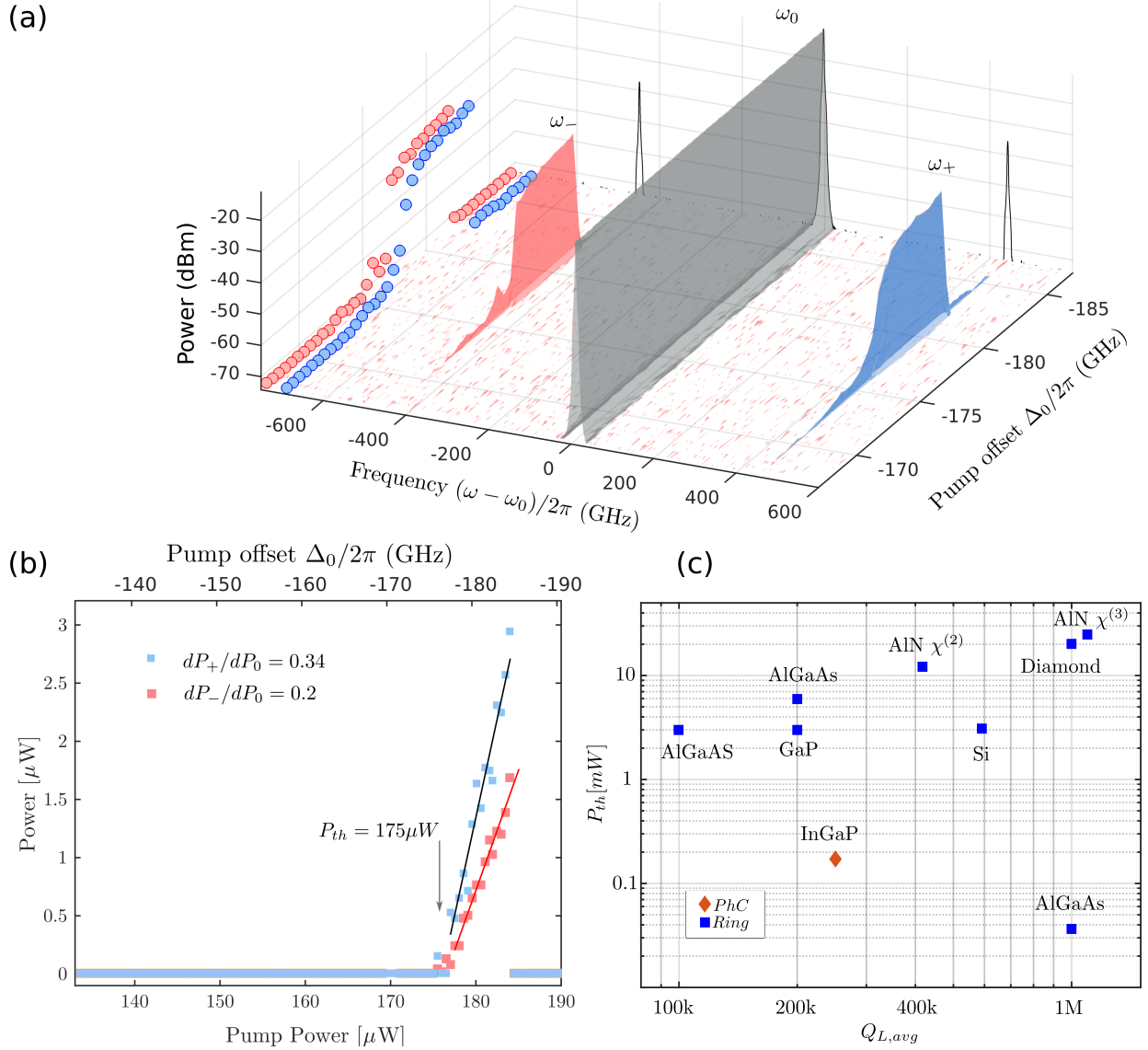


FIG. 3. (a) Parametric oscillation: raw optical spectrum (resolution 4 GHz, centered at the pump frequency) as the pump offset is changed. The threshold is overcome as the intra-cavity pump energy increases. Markers represent the raw power on the red and blue side, solid black line is the spectrum at maximum OPO emission $\Delta_0/2\pi = -183$ GHz; (b) On-chip power in the blue ω_+ and red ω_- lines as a function of the pump offset and equivalent pump power in the cavity $P_{c,0}$; (c) OPO pump threshold as a function of the averaged Q factor Q_{avg} in semiconductor integrated microring and racetrack resonators: AlGaAs[38, 46], GaP[47], Diamond[48], Silicon[49], AlN using $\chi^{(2)}$ [40] and $\chi^{(3)}$ [50] nonlinearity.